Electronic Supplementary Information

Monomeric Fe(III) Half-Sandwich Complexes [Cp'FeX_2] – Synthesis, Properties and Electronic Structure

Matthias Reiners,[a] Miyuki Maekawa,[a] Dirk Baabe,[a] Marc-Kevin Zaretzke,[a] Peter Schweyen,[a] Constantin G. Daniliuc,[a] Matthias Freytag,[a] Jan Raeder,[a] Johannes Hohenberger,[b] Jörg Sutter,[b] Karsten Meyer,[b] and Marc D. Walter*[a]

[a] *Institut für Anorganische und Analytische Chemie, Technische Universität Braunschweig, Hagenring 30, 38106 Braunschweig, Germany*
[b] *University of Erlangen–Nürnberg, Department of Chemistry & Pharmacy, Inorganic Chemistry, Egerlandstr. 1, 91058 Erlangen, Germany.*

Table of content

1. Additional Experimental Details S2
2. Crystallographic Details for Complexes **2**, **3**, **4**, **7** and **8** S4
3. Variable Temperature (VT) ^{1}H NMR Studies S5
4. Solid-state Magnetic Susceptibility of Complexes **2**, **3** and **4** S6
5. Zero-field ^{57}Fe Mössbauer Spectroscopy on Complexes **2**, **6** and **7** S7
6. Electrochemical Studies on Complexes **7** and **8** S10
7. Computational Details S11
8. References S15

1. Additional Experimental Details

[NEt_4][Cp'FeI_2]. A mixture of [Cp'FeI]$_2$ (0.21 g, 0.25 mmol) and NEt_4I (0.13 g, 0.25 mmol) were suspended in CH_2Cl_2 (*ca.* 15 mL). The suspension was stirred at room temperature for 2 h. During this time the reaction mixture turned yellow-orange and a green precipitate formed. The yellow-orange CH_2Cl_2 solution was filtered and a layer of pentane (*ca.* 30 mL) was added. Yellow-orange needles were obtained by slow diffusion at room temperature over 24 h. Yield: 0.21 g (0.31 mmol, 74%). M.p. > 203 °C (dec.). ^{1}H NMR (CD_2Cl_2, 289 K): *δ* 21.0 (8H, NEt_4-C*H*$_2$, $v_{1/2}$= 215 Hz), 11.7 (12H, NEt_4-C*H*$_3$, $v_{1/2}$= 215 Hz), -23.0 (18H, Cp'-C*Me*$_3$, $v_{1/2}$= 220 Hz), -34.9 (9H, Cp'-C*Me*$_3$, $v_{1/2}$= 130 Hz). Anal. calcd. for $C_{25}H_{49}NI_2Fe$ (673.33): C, 44.60; H, 7.34. Found: C, 44.45; H, 7.18.

Reaction of 4 towards H_2 in cyclohexane. Complex **4** (10 mg, 0.02 mmol) was dissolved in cyclohexane-d_{12} (0.7 mL), pressurized with H_2 (8 bar) in an autoclave and stirred at ambient temperatures for 4 h. After releasing the pressure, an 1H NMR spectrum was recorded establishing the formation of complexes **5** and **6** in an approximate ratio of 1:4 besides Me_4Si. For further analytic data of complex **5** and **6** see Ref. [1].

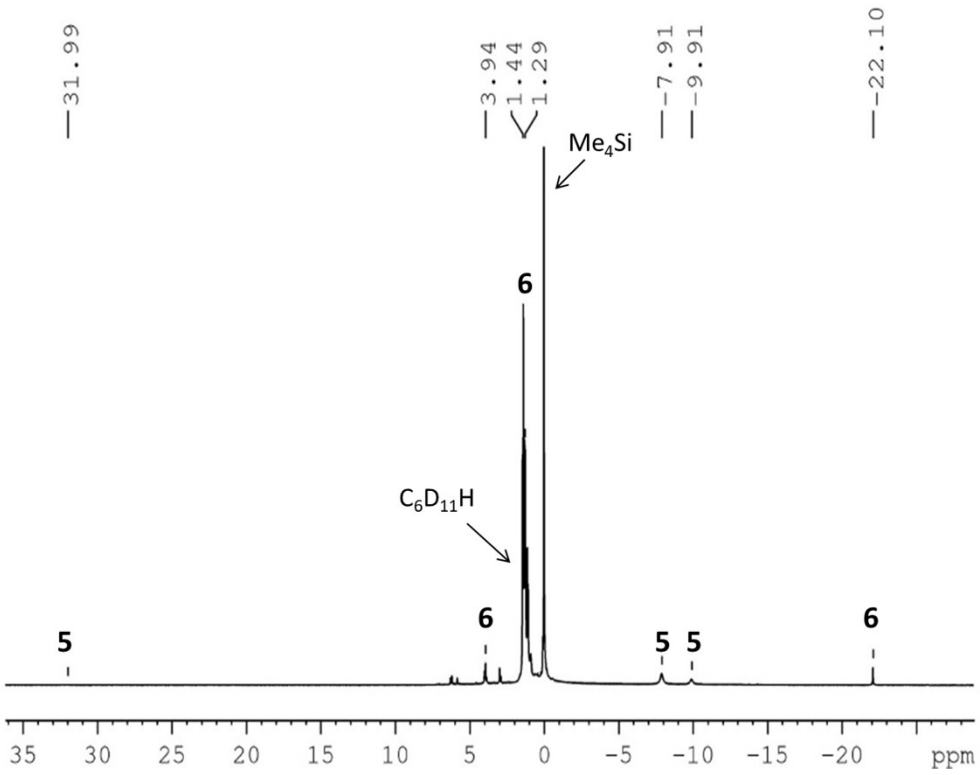

Figure S1. Crude reaction mixture obtained from the hydrogenation of complex **4** in cyclohexane-d_{12}.

[Cp'Fe(μ-H)$_2$]$_2$ (**6**). To a frozen suspension (cooled with liquid N_2) of KC_8 (0.135 g, 1.00 mmol, 2 eq.) and THF (10 mL) in a "bomb" flask (heavy walled flask equipped with a Teflon plug valve) a solution of [Cp'Fe(μ-I)]$_2$ (**1**) (0.416 g, 0.50 mmol, 1 eq.) in THF (10 mL) was added and closed. The frozen flask was taken out of the liquid nitrogen bath and let reach ambient temperature under steering. During

warming to ambient temperature, the suspension turned from light brown over green to a dark brown-violet. After stirring for 2 h the overpressure was carefully released and the solvent in oil pump vacuum removed. The violet brown residue was extracted with hexane (4 x 5 mL) and filtered. After removing the solvent in oil pump vacuum the dark residue was dissolved in a minimum amount of Et_2O (ca. 1 mL) and stored for crystallization at -30°C to give dark violet blocks. Yield: 0.130 g (0.22 mmol, 45%). For further analytical data see Ref. [1].

Reduction of 8 with KC_8. A suspension of KC_8 (6.7 mg, 1.00 eq.) in THF (ca. 5 mL) was added to a stirred solution of **8** (30 mg, 0.05 mmol, 1.00 eq.) in THF (ca. 5 mL) at ambient temperatures and reaction mixture was stirred for an additional 0.5 h. The colour changed immediately from yellow to green. During solvent evaporation under dynamic oil pump vacuum the colour changed to orange. The orange residue was extracted with pentane and dried. The residue was dissolved in a minimum amount of Et_2O and stored at -30°C to yield red blocks of **6** (identification by ^1H NMR spectroscopy and X-ray diffraction analysis). For the UV/vis experiment 7.1mg of **8** was dissolved in THF (50 mL) and filtered over a pad of KC_8. The yellow solution turned immediately green and was directly transferred into a UV/vis cell and measured. The half-life time of **A** at ambient temperature was determined to be ca. 40 min.

2. Crystallographic Details for Complexes 2, 3, 4, 7, and 8

Table S1. Crystallographic data.

Compound	**2**	**3**	**4**	**7**	**8**
Chemical formula	C_{41} H_{66} Fe_2 I_2	C_{17} H_{29} Fe I_2	C_{25} H_{51} Fe Si_2	$C_{46}H_{70}Fe_2$	$C_{23}H_{35}$ $FeSbF_6$
Formula Mass	924.44	543.05	463.69	734.72	603.13
Crystal system	Monoclinic	Orthorhombic	Orthorhombic	Monoclinic	Monoclinic
a/Å	15.2121(2)	12.4512(2)	17.5073(6)	9.64934(15)	10.6190(2)
b/Å	14.6908(2)	17.0538(2)	16.8530(6)	15.7931(2)	12.4220(3)
c/Å	19.0206(4)	18.7165(2)	19.1250(6)	12.94716(16)	18.3035(4)
α/°	90	90	90	90	90
β/°	105.618(2)	90	90	92.1917(12)	92.067(2)
γ/°	90	90	90	90	90
Unit cell volume/Å^3	4093.74(12)	3974.27(9)	5642.8(3)	1971.61(5)	2412.83
Temperature/K	100(2)	100(2)	100(2)	100(2)	100(2)
Space group	*P* 2_1/n	*P* b c a	*P* b c a	*P* 2_1/c	*P* 2_1/c
No. of formula units per unit cell, *Z*	4	8	8	2	4
Radiation type	Mo Kα	Mo Kα	Mo Kα	Cu Kα	Cu Kα
Absorption coefficient, *μ*/mm^{-1}	2.243	3.858	0.628	6.105	14.187
No. of reflections measured	101894	137349	145214	32840	8118
No. of independent reflections	10542	5279	5758	4076	6935
R_{int}	0.0398	0.0392	0.1405	0.0406	-
Final R_1 values ($I > 2\sigma(I)$)	0.0240	0.0160	0.0502	0.0290	0.0497
Final $wR(F^2)$ values ($I > 2\sigma(I)$)	0.0467	0.0319	0.0866	0.0736	0.0568
Final R_1 values (all data)	0.0330	0.0257	0.0955	0.0298	0.1316
Final $wR(F^2)$ values (all data)	0.0499	0.0326	0.0977	0.0741	0.1353
Goodness of fit on F^2	1.074	0.927	1.017	1.044	1.039
Flack parameter	-	-	-	-	-
Largest diff. peak and hole/e Å^3	0.635 / -0.699	0.837 / -0.868	0.481 / -0.295	0.230 / -0.405	1.070 / -2.423

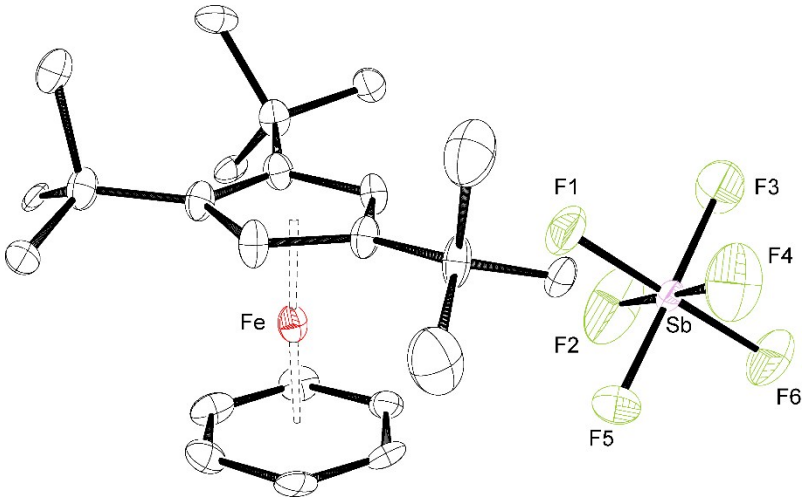

Figure S2. Thermal ellipsoid plot (50% probability) of the molecular structures of complex **8**. H-atoms are omitted for clarity. Disordered positions of the benzene ring and of two *t*Bu-groups are not shown.

3. Variable Temperature (VT) ^{1}H NMR Studies

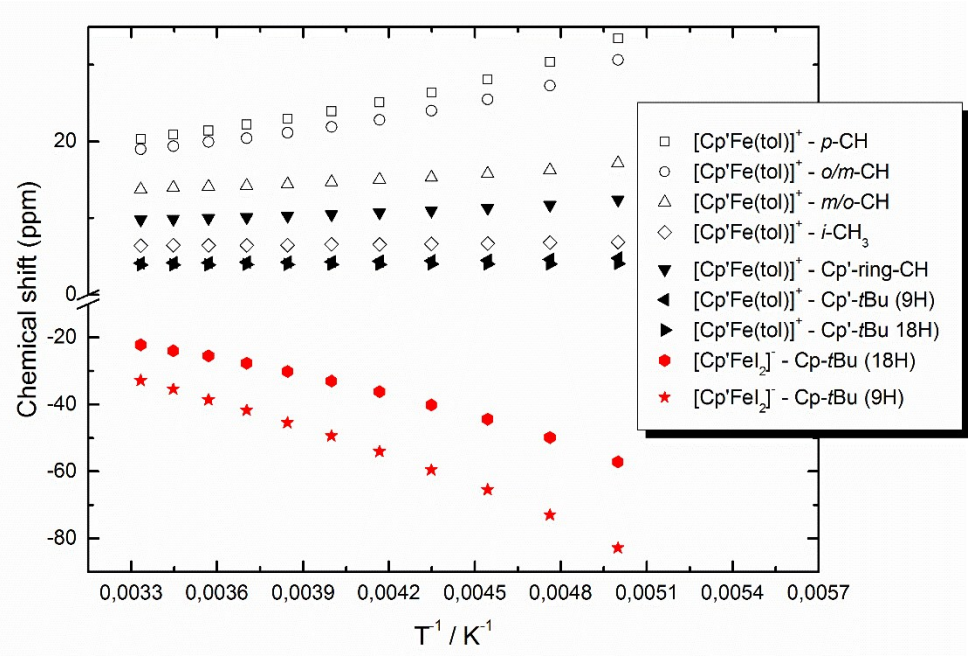

Figure S3. Chemical shift (δ) vs. T^{-1} plot for the ^{1}H NMR resonances of [Cp'Fe(tol)][Cp'FeI$_2$] (**2**) in CD_2Cl_2 between T = 188 and 300 K.

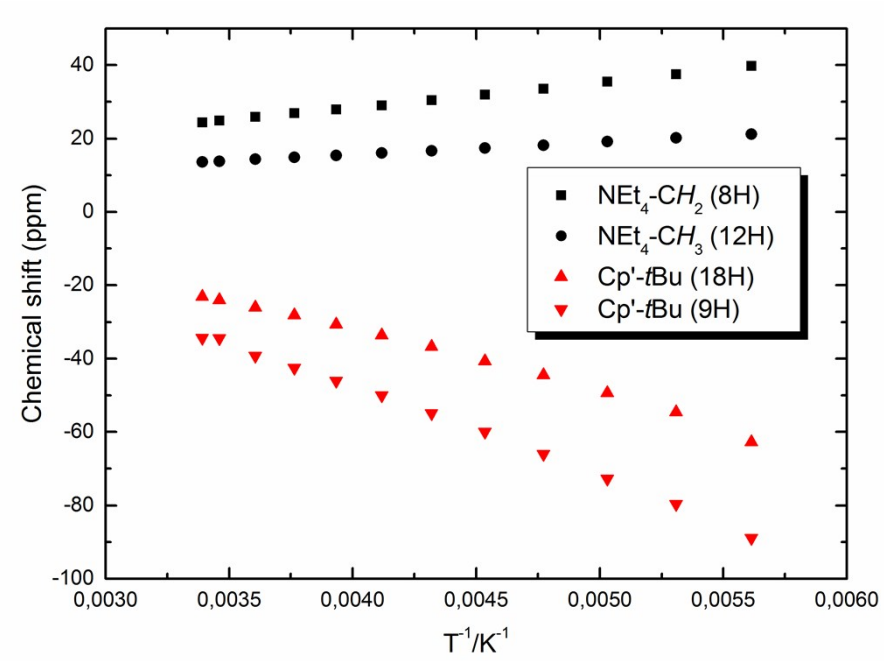

Figure S4. Chemical shift (δ) vs. T^{-1} plot for the ^{1}H NMR resonances of [NEt$_4$][Cp'FeI$_2$] in CD_2Cl_2 between T = 175 and 300 K.

4. Solid-state Magnetic Susceptibility of Complexes 2–4

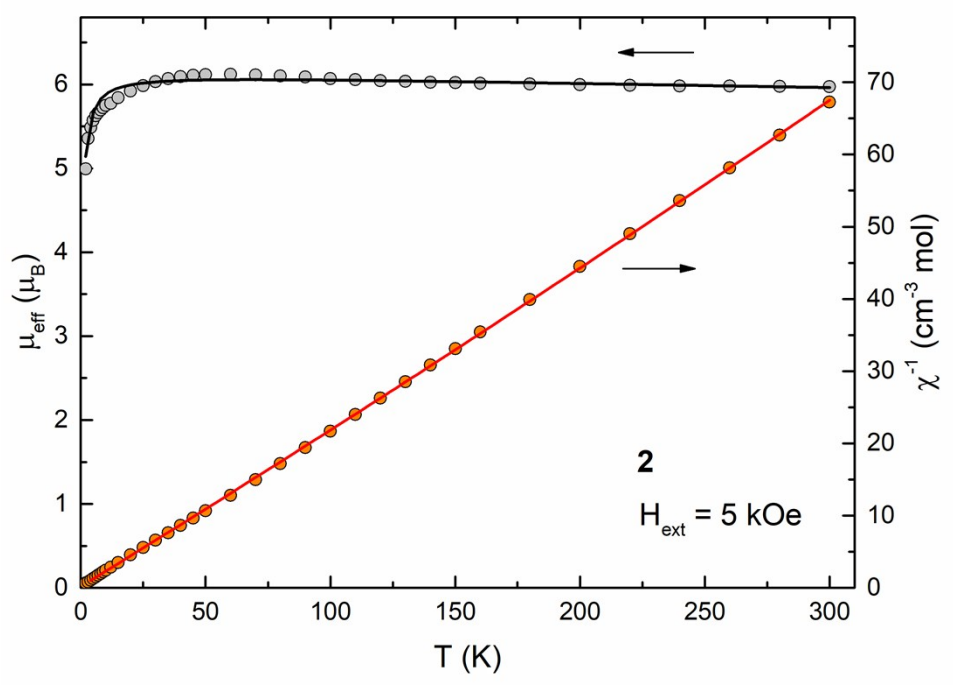

Figure S5. Effective magnetic moment (μ_{eff}) vs. T plot for compound **2,** recorded at temperatures between T = 2.6 and 300 K with an applied magnetic field of H_{ext} = 5 kOe. Symbols: experimental data. Lines: adaptation of a modified Curie-Weiss law (see Table S2).

Table S2. Parameters determined for complexes **2**–**4** using a modified Curie-Weiss model, which considers a phenomenological temperature-independent contribution (χ_{TIP}) to the magnetic susceptibility.

Complex	C (cm^3 K mol^{-1})	θ (K)	χ_{TIP} (10^{-4} cm^3 mol^{-1})	μ_{eff} (μ_B)	Fit
2	4.697(21)	-0.8(2)	-8.0(8)	6.13	
3	2.615(5)	-3.8(2)	-5.2(1)	4.57	T > 50 K
4	2.717(6)	3.7(2)	-6.0(4)	4.66	T > 50 K

5. Zero-field ^{57}Fe Mössbauer Spectroscopy on Complexes 2, 6 and 7

Table S3. Mössbauer parameters for complex **2**. All spectra were analysed by a least-squares fitting routine based on the stochastic relaxation model developed by Blume and Tjon.[2] The isomer shifts (δ_{iso}) were specified relative to metallic iron at room temperature but were not corrected in terms of the second order Doppler shift. The quadrupole splitting is given by $\Delta E_Q = 2\,\varepsilon$ with $\varepsilon = e^2\,q\,Q/4$ and $\eta = 0$ (constants e, q, Q, η were used in their usual meaning). ν_c and V describes the relaxation rate and the population ratio of the two Fe(II) sites, respectively. While the intensity ratio of the second and the third Mössbauer transition ($A_2/A_3 = 2$) was fixed, we phenomenologically used the intensity ratio of the first and the third Mössbauer transition (A_1/A_3) as a free parameter in the fit, that might be explained by texture effects and/or by crystal packing effects (as also observed for complex **7**, *vide infra*).

T	δ_{iso}	ΔE_Q	Γ_{HWHM}	B_{hf}	ν_c	A_1/A_3	A_2/A_3	V	
(K)	(mm s^{-1})	(mm s^{-1})	(mm s^{-1})	(T)	(mm s^{-1})	(1)	(1)	(%)	
150	0.545(5)	-1.672(10)	0.140(8)	0*	-	2.2(1)	2*	51.0	a
	0.976(9)	1.618(16)	0.130(18)	37.4*	182(58)	4.0(4)	2*	49.0	
77	0.561(4)	-1.672(8)	0.141(8)	0*	-	2.2(1)	2*	51.2	a
	1.041(36)	1.688(66)	0.137(25)	37.4*	42.8(8.2)	3.9(6)	2*	48.8	
77	0.551(5)	-1.684(10)	0.138(10)	0*	-	2.3(2)	2*	47.7	b
	0.992(53)	1.638(92)	0.144(36)	37.4*	36.1(7.5)	4.4(9)	2*	52.3	
15	0.558(3)	-1.674(6)	0.157(5)	0*	-	2.3(1)	2*	55.4	b
	1.022(22)	1.474(42)	0.100(16)	37.4*	0.21(16)	4.8(5)	2*	44.6	
12	0.557(4)	-1.682(8)	0.161(6)	0*	-	2.3(1)	2*	54.7	b
	1.024(27)	1.456(52)	0.100(18)	37.4(2)	0.23(18)	4.9(6)	2*	45.3	

[a] Measured with v_{max} = 7.247 mm s^{-1}. [b] Measured with v_{max} = 10.400 mm s^{-1}. (*) Fixed in the simulation.

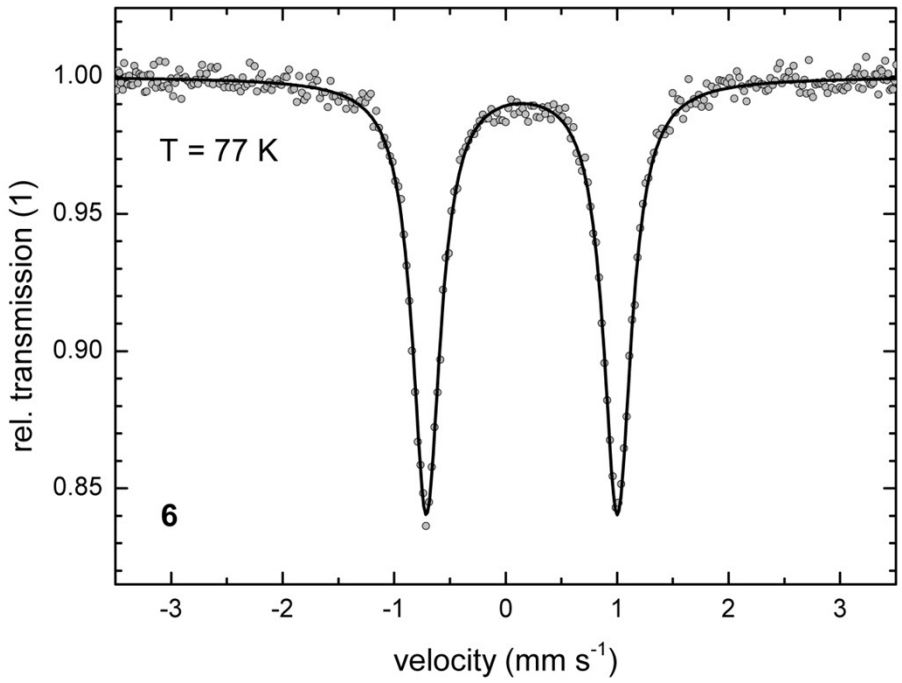

Figure S6. Zero-field ^{57}Fe Mössbauer spectrum for $[Cp'Fe(\mu\text{-}H)_2]_2$ (**6**), recorded at T = 77 K.

Table S4. Mössbauer parameters for complex **6**. The isomer shifts (δ_{iso}) were specified relative to metallic iron at room temperature but were not corrected in terms of the second order Doppler shift. A_-/A_+ describes the intensity ratio of the spectral areas of the low velocity (energy) Mössbauer transition to the high velocity (energy) Mössbauer transition.

T (K)	δ_{iso} (mm s^{-1})	ΔE_Q (mm s^{-1})	Γ_{HWHM} (mm s^{-1})	A_-/A_+ (1)
150	0.241(2)	1.712(3)	0.145(2)	1
77	0.266(2)	1.713(3)	0.153(3)	1
20	0.272(1)	1.713(3)	0.156(2)	1

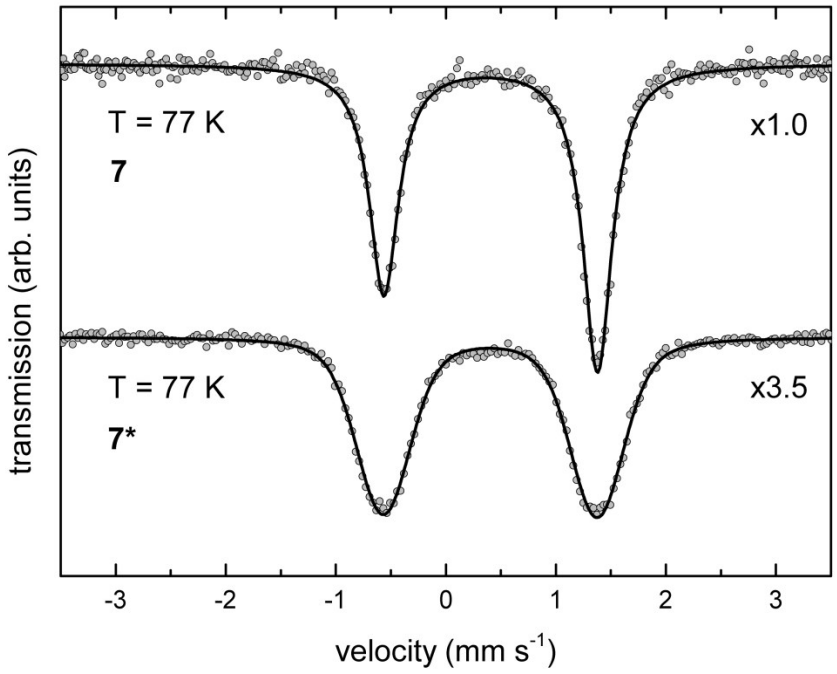

Figure S7. Zero-field ^{57}Fe Mössbauer spectra for [(Cp'Fe)$_2$(μ_2-η^5:η^5-$C_{12}H_{12}$], recorded at T = 77 K on a powdered sample (**7**) or on a frozen THF solution (**7***). This measurement proves that the significantly different peak intensities observed for the doublet in the Mössbauer spectrum of complex **7** are explained by texture effects or by crystal packing effects in this material.

Table S5. Mössbauer parameters for complex **7** and **7***. The isomer shifts (δ_{iso}) were specified relative to metallic iron at room temperature but were not corrected in terms of the second order Doppler shift. A_-/A_+ describes the intensity ratio of the spectral areas of the low velocity (energy) Mössbauer transition to the high velocity (energy) Mössbauer transition.

T (K)	δ_{iso} (mm s^{-1})	ΔE_Q (mm s^{-1})	Γ_{HWHM} (mm s^{-1})	A_-/A_+ (1)
150	0.510(2)	1.935(4)	0.145(3)	0.72(1)
77	0.529(2)	1.941(5)	0.160(3)	0.75(2)
77 [a]	0.524(3)	1.943(5)	0.113(11)	0.99(1)
20	0.537(2)	1.943(4)	0.154(3)	0.77(1)

[a] Recorded in frozen THF solution; the analysis was performed with a doublet of Voigt lines with Gaussian line width σ = 0.194(8) mm s^{-1}.

6. Electrochemical Studies on Complexes 7 and 8

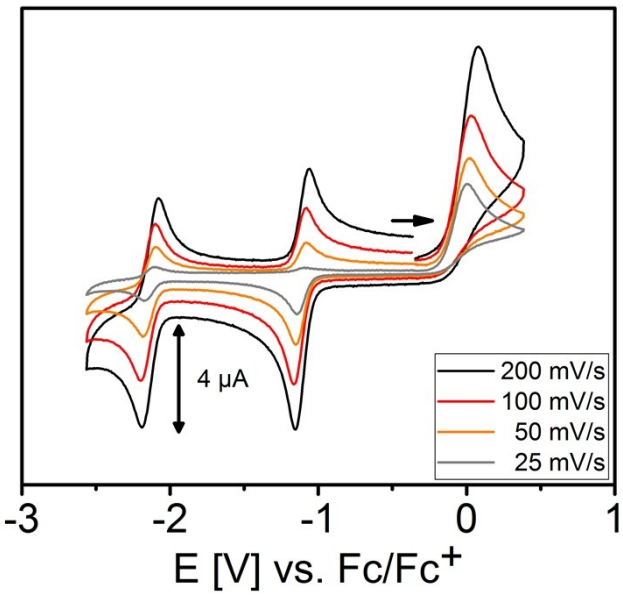

Figure S8. Electrochemical studies performed on complex **7**, recorded at ambient temperatures in THF with 0.1 M [*n*-Bu_4N][PF_6] supporting electrolyte and various scan rates from 25 up to 200 mV s^{-1}: E_{ox} = 0.032 V; $E_{1/2;\ red(1)}$ = -1.121 V; $E_{1/2;\ red(2)}$ = -2.145 V.

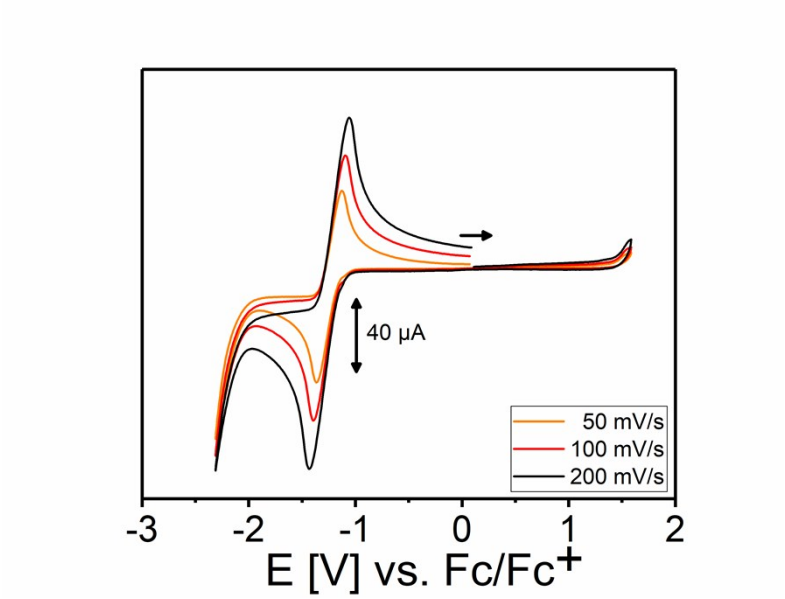

Figure S9. Electrochemical studies performed on complex **8**, recorded at ambient temperatures in THF with 0.1 M [*n*-Bu_4N][PF_6] supporting electrolyte, various scan rates from 50 up to 200 mV s^{-1} and $E_{1/2;\ red}$ = -1.252 V.

7. Computational Details

All computations were performed using the DFT functional method B3LYP as implemented in the Gaussian09 program.[3] The all-electron triple-ζ basis set (6-311G**)[4] was applied for all elements (Fe, Si, C and H), whereas a Stuttgart-Dresden pseudopotential (SDD)[5] was used for iodine (I).

Table S6. Energies of the optimized structures[a]

Compound	E(0 K)[b] [Ha]	H(298 K)[c] [Ha]	G(298 K)[c] [Ha]
	B3LYP:		
$[Cp'FeI_2]^-$ (*S*=0)	-1951.711859 (28.1)	-1951.685305 (27.5)	-1951.767233 (31.3)
$[Cp'FeI_2]^-$ (*S*=1)	-1951.732095 (15.4)	-1951.704816 (15.2)	-1951.790737 (16.5)
[Cp'FeI$_2$]$^-$ (S=2)	***-1951.756644 (0.0)***	***-1951.729062 (0.0)***	***-1951.817027 (0.0)***
$[Cp'FeI_2]$ (*S*=1/2)	-1951.622650 (8.9)	-1951.595876 (8.8)	-1951.678713 (10.1)
[Cp'FeI$_2^-$ (S=3/2)	***-1951.636887 (0.0)***	***-1951.609896 (0.0)***	***-1951.694737 (0.0)***
$[Cp'FeI_2]^-$ (*S*=5/2)	-1951.625422 (7.2)	-1951.597902 (7.5)	-1951.684667 (6.6)
[Cp'Fe(CH$_2$SiMe$_3$)$_2$] (S=3/2)[d]	***-2825.754990 (0.0)***	***-2825.712376 (0.0)***	***-2825.828588 (0.0)***
$[Cp'Fe(CH_2SiMe_3)_2]$ (*S*=5/2)[d]	-2825.722688 (20.3)	-2825.679358 (20.7)	-2825.797311 (19.6)

[a] Values (in kcal/mol) given in parenthesis refer to the energy difference to the lowest computed spin-configuration for the individual compounds. [b] DFT energy incl. ZPE. [c] Standard conditions T = 298.15 K and p = 1 atm. [d]For $[Cp'Fe(CH_2SiMe_3)_2]$ (*S*=1/2) no SCF convergence was achieved.

Table S7. Comparison between computed and experimental structural parameters.

Complex	Cp'_{cent}-Fe (Å)	Fe-X (Å)	X-Fe-X (deg)
$[Cp'FeI_2]^-$ (*S*=0)	1.628	2.701 2.735	95.34
$[Cp'FeI_2]^-$ (*S*=1)	1.825	2.701 2.709	98.22
$[Cp'FeI_2]^-$ (*S*=2)	2.011	2.720 2.765	106.70
$[Cp'FeI_2]^-$ (exp)	1.99	2.6168(3) 2.7027(3)	102.104(10)
$[Cp'FeI_2]$ (*S*=1/2)	1.717	2.564 2.600	99.11
$[Cp'FeI_2]$ (*S*=3/2)	1.874	2.574 2.591	104.90
$[Cp'FeI_2]$ (*S*=5/2)	1.993	2.603 2.630	108.40
$[Cp'FeI_2]$ (exp)	1.86	2.5154(2) 2.5238(2)	103.725(9)
$[Cp'Fe(CH_2SiMe_3)_2]$ (*S*=3/2)	1.971	2.011 2.015	98.05
$[Cp'Fe(CH_2SiMe_3)_2]$ (*S*=5/2)	2.162	2.048 2.069	113.01
$[Cp'Fe(CH_2SiMe_3)_2]$ (exp)	1.91	1.998(2) 2.0016(19)	98.57(9)

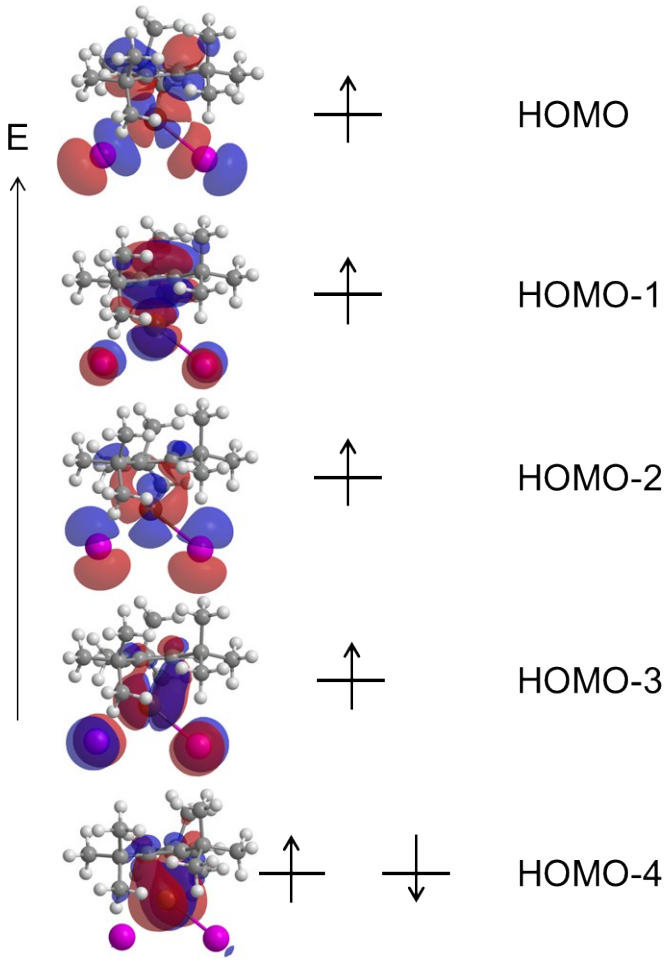

Figure S10. (Biorthogonalized) Kohn-Sham molecular orbitals for $[Cp'FeI_2]^-$ anion from complex (**2**).

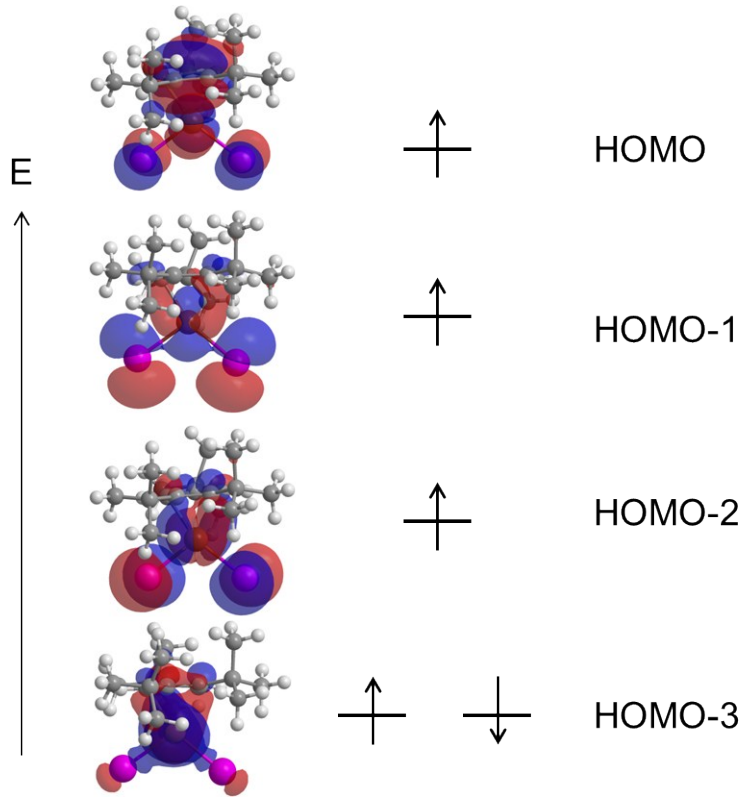

Figure S11. (Biorthogonalized) Kohn-Sham molecular orbitals for [Cp'FeI_2] (**3**).

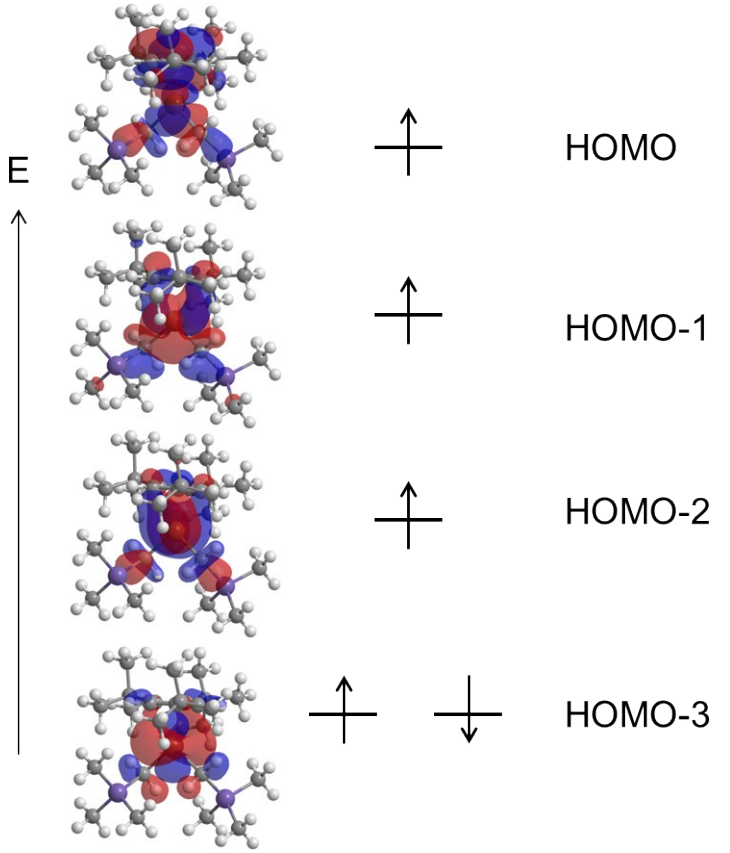

Figure S12. (Biorthogonalized) Kohn-Sham molecular orbitals for [Cp'$Fe(CH_2SiMe_3)_2$] (**4**).

8. References

[1] M. D. Walter, J. Grunenberg and P. S. White, *Chem. Sci.* 2011, **2**, 2120-2130.

[2] M. Blume and J. A. Tjon, *Phys. Rev.*, 1968, **165**, 446-456.

[3] Gaussian 09, Revision A.1, M. J. Frisch, G. W. Trucks, H. B. Schlegel, G. E. Scuseria, M. A. Robb, J. R. Cheeseman, G. Scalmani, V. Barone, B. Mennucci, G. A. Petersson, H. Nakatsuji, M. Caricato, X. Li, H. P. Hratchian, A. F. Izmaylov, J. Bloino, G. Zheng, J. L. Sonnenberg, M. Hada, M. Ehara, K. Toyota, R. Fukuda, J. Hasegawa, M. Ishida, T. Nakajima, Y. Honda, O. Kitao, H. Nakai, T. Vreven, J. A. Montgomery, Jr., J. E. Peralta, F. Ogliaro, M. Bearpark, J. J. Heyd, E. Brothers, K. N. Kudin, V. N. Staroverov, R. Kobayashi, J. Normand, K. Raghavachari, A. Rendell, J. C. Burant, S. S. Iyengar, J. Tomasi, M. Cossi, N. Rega, J. M. Millam, M. Klene, J. E. Knox, J. B. Cross, V. Bakken, C. Adamo, J. Jaramillo, R. Gomperts, R. E. Stratmann, O. Yazyev, A. J. Austin, R. Cammi, C. Pomelli, J. W. Ochterski, R. L. Martin, K. Morokuma, V. G. Zakrzewski, G. A. Voth, P. Salvador, J. J. Dannenberg, S. Dapprich, A. D. Daniels, Ö. Farkas, J. B. Foresman, J. V. Ortiz, J. Cioslowski, and D. J. Fox, Gaussian, Inc., Wallingford CT, 2009.

[4] X. Cao and M. Dolg, *J. Chem. Phys.* 2001, **115**, 7348.

[5] A. Bergner, M. Dolg, W. Küchle, H. Stoll and H. Preuss, *Mol. Phys.* 1993, **80**, 1431-41.